

# Commissural Neurons in the Rat Ventral Cochlear Nucleus

JOHN R. DOUCET<sup>1</sup>, NICOLE M. LENIHAN<sup>1</sup>, AND BRADFORD J. MAY<sup>1</sup>

<sup>1</sup>Center for Hearing and Balance, Department of Otolaryngology—Head and Neck Surgery, Johns Hopkins University School of Medicine, Traylor Research Building, Room 521, 720 Rutland Avenue, Baltimore, MD 21205, USA

Received: 5 June 2008; Accepted: 30 December 2008; Online publication: 27 January 2009

## ABSTRACT

Commissural neurons connect the cochlear nucleus complexes of both ears. Previous studies have suggested that the neurons may be separated into two anatomical subtypes on the basis of percent apposition (PA); that is, the percentage of the soma apposed by synaptic terminals. The present study combined tract tracing with synaptic immunolabeling to compare the soma area, relative number, and location of Type I (low PA) and Type II (high PA) commissural neurons in the ventral cochlear nucleus (VCN) of rats. Confocal microscopic analysis revealed that 261 of 377 (69%) commissural neurons have medium-sized somata with Type I axosomatic innervation. The commissural neurons also showed distinct topographical distributions. The majority of Type I neurons were located in the small cell cap of the VCN, which serves as a nexus for regulatory pathways within the auditory brainstem. Most Type II neurons were found in the magnocellular core. This anatomical dichotomy should broaden current views on the function of the commissural pathway that stress the fast inhibitory interactions generated by Type II neurons. The more prevalent Type I neurons may underlie slow regulatory influences that enhance binaural processing or the recovery of function after injury.

**Keywords:** binaural hearing, commissural pathways, regulatory pathways, multipolar cells, stellate cells, deconvolution

## INTRODUCTION

Commissural neurons in the cochlear nucleus (CN) allow direct communications between the cochlear nuclei (Cant and Gaston 1982). An understanding of the functional relevance of these projections has been limited by an incomplete description of the principal cell types that contribute to the anatomical connections. Alibardi (1998) classified commissural neurons in the ventral cochlear nucleus (VCN) by somatic morphology. The key distinguishing anatomic feature was percent apposition (PA), which is the percentage of the soma that is contacted by synaptic terminals (Cant 1981). Type I neurons have low PA (few axosomatic terminals), while Type II neurons have high PA (many axosomatic terminals).

The existence of Types I and II neurons implies that the commissural pathway may perform multiple sound-processing roles. This interpretation is supported by the distinct electrophysiological properties that have been attributed to VCN multipolar cells (commissural neurons are a subset of multipolar cells) with Type I versus Type II morphologies (Smith and Rhode 1989). The Type II morphology (high PA) is a definitive anatomical feature of D-stellate multipolar neurons (Smith and Rhode 1989; Oertel et al. 1990; Doucet and Ryugo 1997). Tract-tracing studies have confirmed that these neurons project to the contralateral cochlear nucleus (Arnott et al. 2004; Smith et al. 2005; Doucet and Ryugo 2006). Because Type II (D-stellate) neurons are glycinergic (Wenthold 1987; Alibardi, 1998; Doucet et al. 1999), they are thought to be a major source of the short-latency inhibition that is observed in the cochlear nucleus after contralateral stimulation (Pfalz 1962; Mast 1970; Young and Brownell 1976; Babalian et al. 1999; Needham and Paolini 2003; Shore et al. 2003). However, the majority of commissural neurons lack

---

Correspondence to: Bradford J. May • Center for Hearing and Balance, Department of Otolaryngology—Head and Neck Surgery • Johns Hopkins University School of Medicine • Traylor Research Building, Room 521, 720 Rutland Avenue, Baltimore, MD 21205, USA. Telephone: +1-410-6141878; fax: +1-410-9551299; e-mail: bmay@jhu.edu

the anatomical features that are characteristic of the Type II morphology (Shore et al. 1992; Schofield and Cant 1996b; Alibardi 1998; Doucet and Ryugo 2006).

In light of Alibardi's findings (1998), we hypothesized that Type I neurons are the dominant source of VCN commissural projections. The present study investigated the relative strength of Types I and II components by identifying commissural neurons with contralateral cochlear nucleus injections of the retrograde tracer Fluorogold (FG). The axosomatic contacts of FG-labeled neurons were visualized by attaching a fluorescent tag to SV2 (a ubiquitous synaptic vesicle protein) via immunohistochemistry. The PA score of a commissural neuron was estimated by quantifying the percentage of the FG-labeled soma apposed by SV2-immunofluorescence—a light microscopic definition of PA analogous to the EM metric defined by Cant (1981). The analysis of 377 commissural neurons revealed 261 (69%) neurons with PA scores that were indicative of the Type I morphology. Our findings suggest that the functional role of the VCN commissural pathway extends beyond the fast inhibitory influences of the less abundant Type II projections.

## METHODS

The present report is based on data obtained from three male Sprague–Dawley rats weighing between 300 and 380 g. All animals were used in accordance with National Institutes of Health guidelines and the approval of the Animal Care and Use Committee for The Johns Hopkins University School of Medicine.

### Surgery and tracer injection

Rats were anesthetized with isoflurane followed by sodium pentobarbital (50 mg/kg, i.p.). The surgical area was treated with subcutaneous injections of lidocaine (total volume of 1 cm<sup>3</sup>). The left CN was exposed by reflecting overlying muscles, opening the skull, and partially aspirating the cerebellum.

A glass micropipette (inner tip diameter=40–50 μm) was positioned in the CN with a stereotaxic instrument. At several depths along multiple penetrations, a nanoliter injector dispensed 14 nl of FG tracer (Biotium, Inc., Hayward, CA, USA; 3% solution in distilled water). The injection strategy was to maximize the number of labeled commissural neurons in the right cochlear nucleus by completely filling the left cochlear nucleus.

The brain cavity was packed with gel foam, the surgical incision closed with wound clips, and buprenorphine was administered as a postoperative analgesic (0.05 mg/kg, i.m.). Rats recovered from anesthesia

in a warm room before being returned to institutional animal housing facilities.

At least 6 days after surgery, the rats were euthanized with sodium pentobarbital (100 mg/kg) and then perfused through the heart with fixative (4% paraformaldehyde in 0.1 M phosphate buffer, pH 7.4). Brains were removed, halved at the midline, and cryoprotected by placing them in a 30% sucrose solution (made in phosphate buffer) at 4°C for at least 2 days.

### Tissue processing and data analysis

**Defining the FG injection site.** Tissue containing the left cochlear nucleus was frozen and cut into 50-μm coronal sections on a sliding microtome. The sections were mounted on Superfrost Plus slides (Fisher Scientific), coverslipped with Vectashield Hardset mounting medium (Invitrogen-Molecular Probes, Carlsbad, CA, USA), and stored at 4°C.

The cochlear nucleus was photographed with a Microfire color digital camera (Optronics; Goleta, CA, USA) that was coupled to a Nikon E600 microscope. Background fluorescence was defined by centering the field-of-view of a ×10 objective (NA=0.45) over the tissue section but outside the injection site. The camera's exposure time was adjusted until the median of all pixel values was just greater than zero. These parameters were held constant for subsequent photography.

A photomontage of the injection site was acquired by stitching together multiple fields-of-view. The images were acquired with software that controlled the movements of a motorized microscope stage (Virtual Slice plugin for NeuroLucida; MicroBrightfield Inc.; Essex, VT, USA). The photomontage was converted to gray scale and exported to Adobe Photoshop (version 9). The borders of the cochlear nucleus were traced, and a threshold criterion (×5 background fluorescence) was used to identify labeled pixels.

In all three rats, the injection site almost completely filled the DCN and posterior VCN. The extent of the AVCN injection varied across rats (Fig. 1). The injection site also involved fiber tracts surrounding the cochlear nucleus, which include the inferior cerebellar peduncle, the trapezoid body, and the vestibular nerve. Because contralateral projections into or near these tracts originate exclusively from commissural neurons, the spread of the injection site did not generate artifactual labeling in the right cochlear nucleus.

**Immunohistochemistry.** The right cochlear nucleus was embedded in Neg50 (Richard-Allen Scientific; Kalamazoo, MI, USA), rapidly frozen using methylbutane cooled to –80°C, and cut into 4-μm coronal sections on a cryostat (Microm HM560M

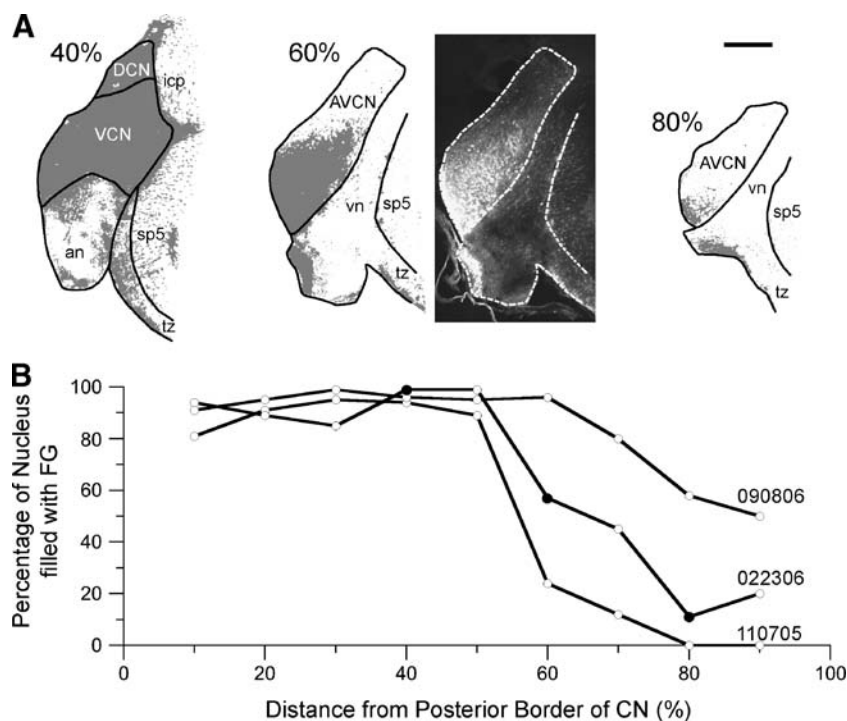


**FIG. 1.** Fluorogold (FG) injection sites. **A.** Three coronal sections through the injection site of rat 022306. Percentages refer to the location of each section along the anterior–posterior axis of the cochlear nucleus (0% equals the posterior border). A photomontage of the injection site was converted to a binary image by applying a threshold procedure. Gray indicates pixels where fluorescence exceeded threshold. The binary image was then superimposed on

the borders of the cochlear nucleus. For one location (60%), both the binary image and photomontage are shown. Scale bar=500  $\mu$ m. an auditory nerve; icp inferior cerebellar peduncle; sp5 spinal trigeminal tract; tz trapezoid body; vn vestibular nerve. **B** Distribution of FG label along the anterior–posterior axis of the injected cochlear nucleus. Closed circles identify data from images that are shown above the plot.

Cryo-star). Thicker tissue sections resulted in poor antibody penetration.

Serial sections were collected on Superfrost Plus slides and saved in blocks of 20. Because the thin sections were fragile, some were irretrievably damaged. On average, 16 out of every 20 sections were captured. The tissue was stored with desiccant at  $-20^{\circ}\text{C}$ .

The VCN extended across 25–30 blocks (approximately 450 captured sections). Eight blocks representing all regions of the VCN were selected for immunohistochemical analyses. The PA score was estimated for all FG-labeled somata that were found within the first ten sections of every selected block.

After being washed in Tris-buffered saline (TBS, 0.05 M, pH 7.4), selected sections were encircled with a PAP pen and then incubated for 1 h at  $21^{\circ}\text{C}$  in a blocking solution (T-TBS: TBS that contains 0.1% Triton X-100 and 5% normal goat serum, Chemicon, Temecula, CA, USA). Next, they were placed overnight in a humid chamber at  $4^{\circ}\text{C}$  in T-TBS containing rabbit anti-FG (1:20,000; Chemicon, catalog no.: AB153) and mouse anti-SV2 (1:1,000; Developmental Studies Hybridoma Bank, University of Iowa). The following day, they were incubated for 1.5 h at  $21^{\circ}\text{C}$  in T-TBS that contained goat anti-rabbit conjugated to Alexafluor 594 (1:1000; Invitrogen-Molecular Probes)

and goat anti-mouse conjugated to biotin (1:1000; Jackson ImmunoResearch Laboratories, West Grove, PA, USA). After several washes in TBS, the slides were placed in a humid chamber and incubated overnight at  $4^{\circ}\text{C}$  in T-TBS containing streptavidin conjugated to Alexafluor 488 (1:10,000; Invitrogen-Molecular Probes). In the morning, after several washes in TBS, the slides were air-dried, coverslipped with Vectashield Hardset mounting medium with DAPI, and stored at  $4^{\circ}\text{C}$ .

Independent studies have confirmed the specificity of SV2 immunoreactivity (SV2-ir). The anti-SV2 monoclonal antibody reacts with all known SV2 isoforms but not with other synaptic or neural proteins (Buckley and Kelly 1985; Bajjalieh et al. 1994; Janz and Sudhof 1999). Immunodetection of SV2 is a standard method for marking synaptic terminals in the brain (Nealen 2005; Brooke et al. 2006). It also has been unambiguously associated with synaptic vesicles in presynaptic terminals by EM studies of the rat brain (Buckley and Kelly 1985).

The following observations and control procedures provide further documentation of immunolabeling specificity. No FG immunoreactivity (FG-ir) was observed in tissue sections obtained from uninjected rat brains. Intense SV2-ir was observed in the cochlear



nucleus but not surrounding fiber tracts (Fig. 2). High-magnification views of the cochlear nucleus revealed SV2-ir profiles with well-defined borders and morphologies (Fig. 2A–G). These patterns of SV2-ir match labeling patterns previously published using antibodies directed against other synaptic vesicle proteins such as synaptophysin (Benson et al. 1997; Muly et al. 2002). Deletion of primary or secondary antibodies, either one at a time or in combination, removed the labeling of the appropriate epitope(s) and produced no evidence of cross-reactivity.

As hypothesized, VCN commissural neurons were heterogeneous with respect to PA (Fig. 2A–G). Two observations lend confidence that variations in the amount of SV2-ir surrounding commissural neurons reflect the true nature of axosomatic innervation and not the quality of immunolabeling. First, somata encircled by SV2-ir (Fig. 2A and E) and those apposed by little SV2-ir (Fig. 2C, D, and F) were frequently observed within a few microns of each other (Fig. 2D and E). Second, the amount of SV2-ir apposed to the soma was similar for two pieces of the same neuron in adjacent sections (Fig. 2A vs. B and F vs. G).

**Confocal microscopy.** Photomicrographs of immunofluorescent labeling were acquired with a laser scanning confocal microscope (Zeiss LSM 510 Meta). The DAPI fluorophore was excited with a diode laser (405 nm). Alexafluor 488 was excited with an argon laser (laser lines of 458, 477, 488, and 514 nm) and Alexafluor 594 with a HeNe laser (562 nm). Separate channels were used to detect the light simultaneously emitted by each fluorophore. Laser power and emission filters were adjusted so that the bleed-through artifact of each emission was undetectable when the lasers of the other two channels were turned off.

For each section in the selected tissue sample, the field-of-view of a  $\times 20$  objective (NA=0.75) was centered over the cochlear nucleus. The confocal pinhole was adjusted to ensure that all emitted light was detected. Then, with the Zeiss software controlling the motorized microscope stage, several different fields-of-view were stitched together to produce a low-magnification photomontage (Fig. 2, sections 1 and 2).

The low-magnification images served two purposes. First, they marked stage coordinates so that FG-labeled somata could be quickly centered in the restricted field

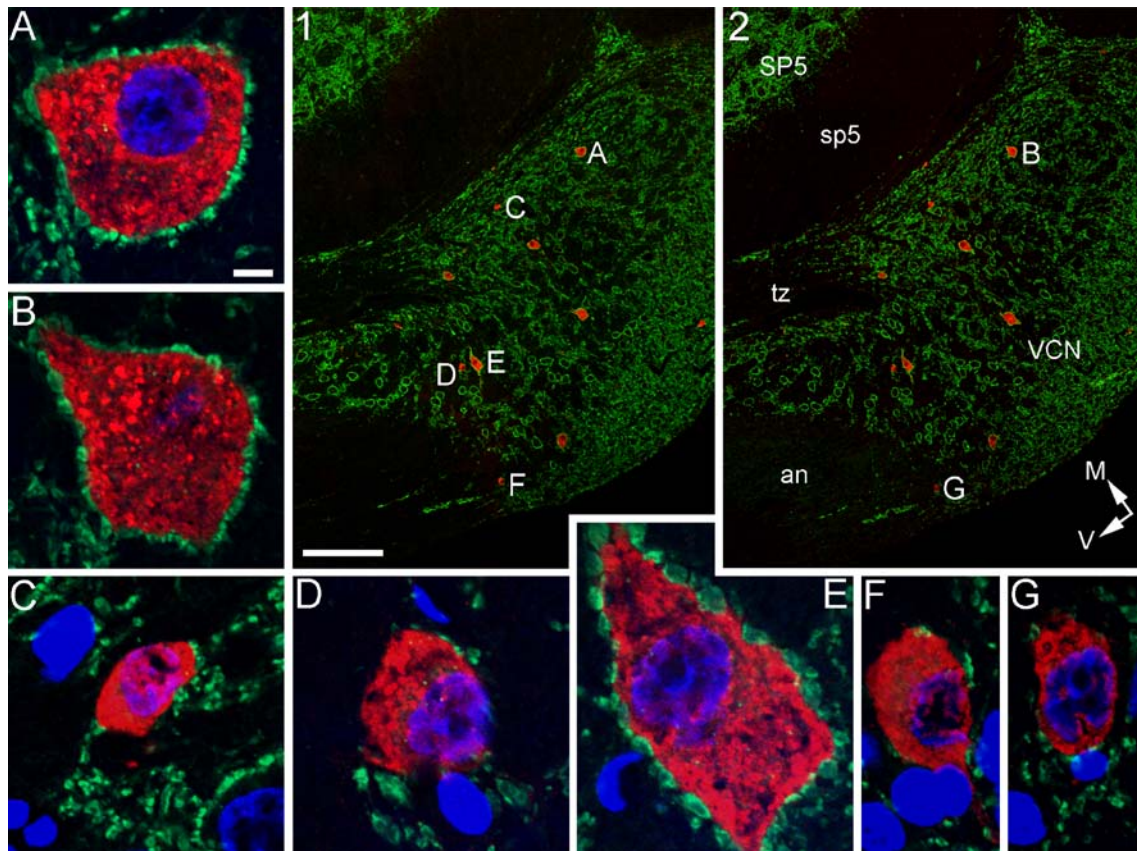


**FIG. 2.** Confocal microscopic images of FG-ir (red), SV2-ir (green), and DAPI labeling (blue) in the right VCN. Sections 1 and 2. Low-magnification photomontages of adjacent coronal sections. DAPI labeling is not shown. Scale bar=200  $\mu$ m.

nucleus. A–G. High-magnification images of representative FG-labeled neurons from sections 1 and 2. Each image is a single optical slice (0.7  $\mu$ m) before deconvolution. Scale bar=5  $\mu$ m.

of a high-powered lens ( $\times 63$ ). Second, they facilitated offline comparisons of adjacent tissue sections to confirm that all labeled somata were analyzed once and none were analyzed twice (e.g., Fig. 2A and B).

Each labeled soma was photographed using a  $\times 63$  lens (NA=1.4). The  $512 \times 512$  pixel images were collected with an electric zoom of  $\times 4$  and saved with 12-bit resolution. Gain and offset were adjusted to optimize signal-to-noise ratios within each emission channel while also making sure that all pixel values fell within the dynamic range of the photodetector. Labeling was sampled through the depth of each section by making optical slices with a thickness of  $0.7 \mu\text{m}$  and a separation

of  $0.2 \mu\text{m}$ . The optical slices associated with each labeled soma will be referred to as a z-stack.

**Measuring soma area and percent apposition.** Each z-stack was deconvolved using the 3D-blind deconvolution algorithm (Autodeblur Gold CWF vX1.3.3; Media Cybernetics; Silver Spring, MD, USA). Deconvolution enhanced the accuracy of PA scores by increasing the effective resolution of spatial coordinates (Fig. 3).

Three consecutive optical slices containing the nucleus of the cell body were cropped from the z-stack and merged. The procedures for deriving soma area (SA) and PA from the merged image

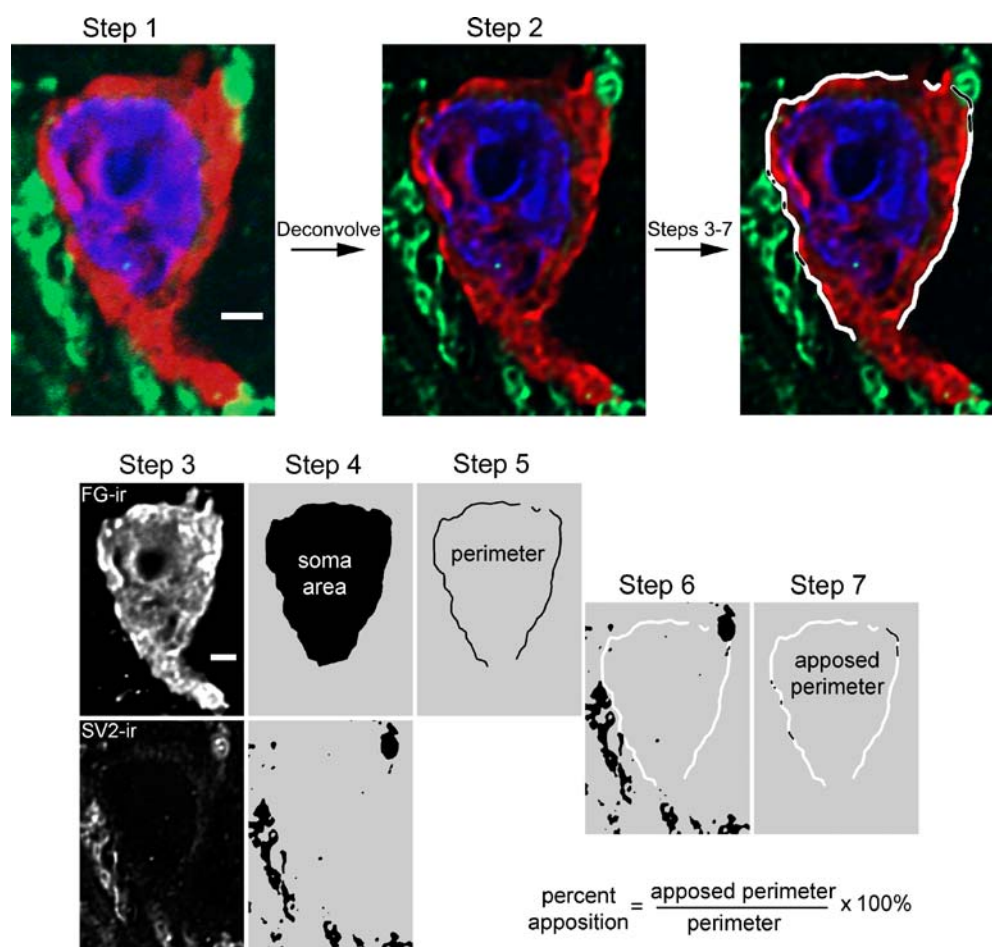


**FIG. 3.** Image acquisition and processing steps used to measure soma area and percent apposition. **Step 1** A z-stack was captured through each FG-labeled neuron with a confocal microscope. The image shows the maximum projection of each channel for three consecutive optical slices through the nucleus. *Scale bar* equals  $2 \mu\text{m}$  and applies to top three panels. **Step 2** Z-stacks were deconvolved offline. The improved resolution obtained with deconvolution is observed by comparing this image with that shown in **Step 1** (maximum projection of the same three optical slices, identical adjustments to brightness, and contrast applied to both images). **Step 3** *Gray-scale images* of FG-ir and SV2-ir obtained from **Step 2** were exported to Photoshop. *Scale bar* equals  $2 \mu\text{m}$  and applies to panels in **steps 3–7**. **Step 4** FG-ir: soma

area was measured after tracing the perimeter of the cell body. SV2-ir: a threshold was used to distinguish between regions that were immunolabeled (*black pixels*) and those that were not (*gray pixels*). **Step 5** FG-ir: the perimeter of the soma was measured after first erasing pieces within dendrites. **Step 6** FG-ir: a search region (*white pixels*) was created that was  $350 \text{ nm}$  wide when measured perpendicular to each point along the perimeter. SV2-ir within the search region was defined as being apposed to the soma. **Step 7** Pieces of the perimeter that were NOT apposed by SV2-ir were erased so that we could measure the apposed perimeter (*black lines in search region*). At the top of the figure, the search region and apposed perimeter are overlaid on the image from **Step 2**.

are illustrated in Figure 3. As previously observed in the cerebellum (Buckley and Kelly 1985), weak SV2-ir was detected inside the soma of most CN neurons. A threshold procedure was used to distinguish SV2-ir signal from background. The threshold for each neuron was set just above the maximum fluorescence within the soma, ignoring isolated and very bright pixels caused by nonspecific adhesion of the fluorophore.

**Cluster analysis.** Commissural neurons may be divided into two subpopulations based on correlations between SA and PA scores (Fig. 4). The *k*-means clustering algorithm (implemented as the *kmeans* function in MATLAB) provided an objective method for classifying these morphological features. Although the number of clusters (*k*) is only constrained by sample size, two clusters were used to test the generalization of Alibardi's (1998) Type I versus Type II classification scheme to the present dataset.

A detailed description of the mathematical calculations performed by the *kmeans* function may be obtained directly from MATLAB documentation. Briefly, SA and PA scores were normalized to the largest value in each data set to remove differences in scale. Neurons were randomly assigned to one of the two clusters. The center of each cluster was defined by computing the mean SA and PA score for all neurons in the cluster. Euclidian distances were compared between individual neurons and the two cluster centers. Neurons were reassigned to the nearest cluster and the measures repeated until there were no further reassignments.

## RESULTS

The SA and PA scores of commissural neurons were highly variable (Figs. 2 and 4). Somata could be very small (Fig. 2C, filled arrowhead in Fig. 4) or giant-sized (Fig. 2E, open arrowhead in Fig. 4). Some somata were covered with synaptic terminals and yielded PA scores

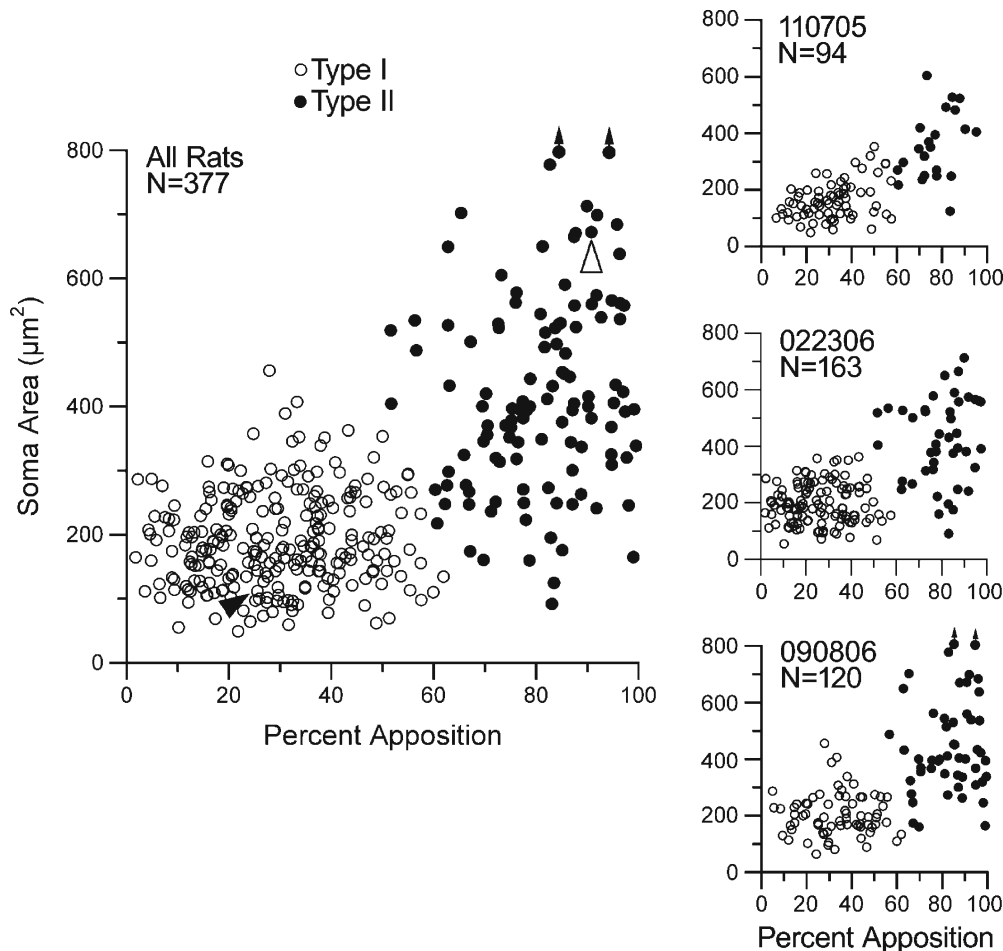


**FIG. 4.** Scatterplots of *Percent Apposition* and SA for the complete sample of VCN commissural neurons. Data from individual rats are presented in the *right panels*. Each *symbol* represents one neuron. *Arrows* identify two neurons with SA scores greater than  $900 \mu\text{m}^2$ . These outliers are plotted at the upper axis limit. *Closed and open arrowheads* in the left scatterplot identify the neurons in Figure 2C and E, respectively.



greater than 90% (Fig. 2E). Others received few synaptic terminals and produced scores less than 25% (Fig. 2C). Between these extremes, SA and PA scores formed continuous distributions.

The statistical patterns of morphological features in the present study were consistent with previous SA measures (Shore et al. 1992). They departed from EM-based descriptions of axosomatic innervation (Alibardi 1998) that suggest a sharp dichotomy between the low PA Type I neurons (20–40%) and the high PA Type II neurons (65–85%). Sample size may contribute to this difference. The present LM analysis was applied to 377 commissural neurons, while the EM analysis of Alibardi was limited to 70 neurons.

### Classification of commissural neurons

The present distribution of PA scores (Fig. 5A) shows a bimodal polarity that is reminiscent of the dual categorization proposed by Alibardi (1998). Partition of the dataset was motivated further by a shared association between PA and SA scores. Specifically, neurons with low PA scores tended to have low SA scores (Fig. 4).

The k-means clustering algorithm was used to classify commissural neurons on the basis of their PA and SA scores. Two partitions were used in the analysis, following the convention established by Alibardi's Types I and II categories. The outcome of the classification is shown in Figure 4. In keeping with Alibardi's terminology, the low PA–low SA cluster was designated Type I. These neurons exhibited a mean PA score of 29% ( $\pm 13.6\%$ , SD) and a mean SA score of  $191 \mu\text{m}^2$  ( $\pm 74 \mu\text{m}^2$ , SD). The high PA–high SA cluster was designated Type II. These neurons produced a mean PA score of 81% ( $\pm 11\%$ ) and a mean SA score of  $419 \mu\text{m}^2$  ( $\pm 162 \mu\text{m}^2$ ).

The anatomical properties of the statistically derived clusters agree with previously published descriptions. The mean PA scores for Types I and II clusters closely match those reported in the Alibardi study (see arrows in Fig. 5A). The SA scores of D-stellate or Type II commissural neurons also have been published (Doucet and Ryugo 2006). Although their sample of D-stellate or Type II commissural neurons was obtained with different methods, the anatomical variation reported by Doucet and Ryugo ( $418 \pm 140 \mu\text{m}^2$ ,  $N=50$ ) is virtually identical to the distribution of SA scores within the Type II cluster (see arrow in Fig. 5B).

### Relative number of Types I and II neurons

The sample of commissural neurons showed a preponderance of the Type I morphology (261/377 neurons, 69%). The Type I bias was observed in the combined data of all three rats and in the individual

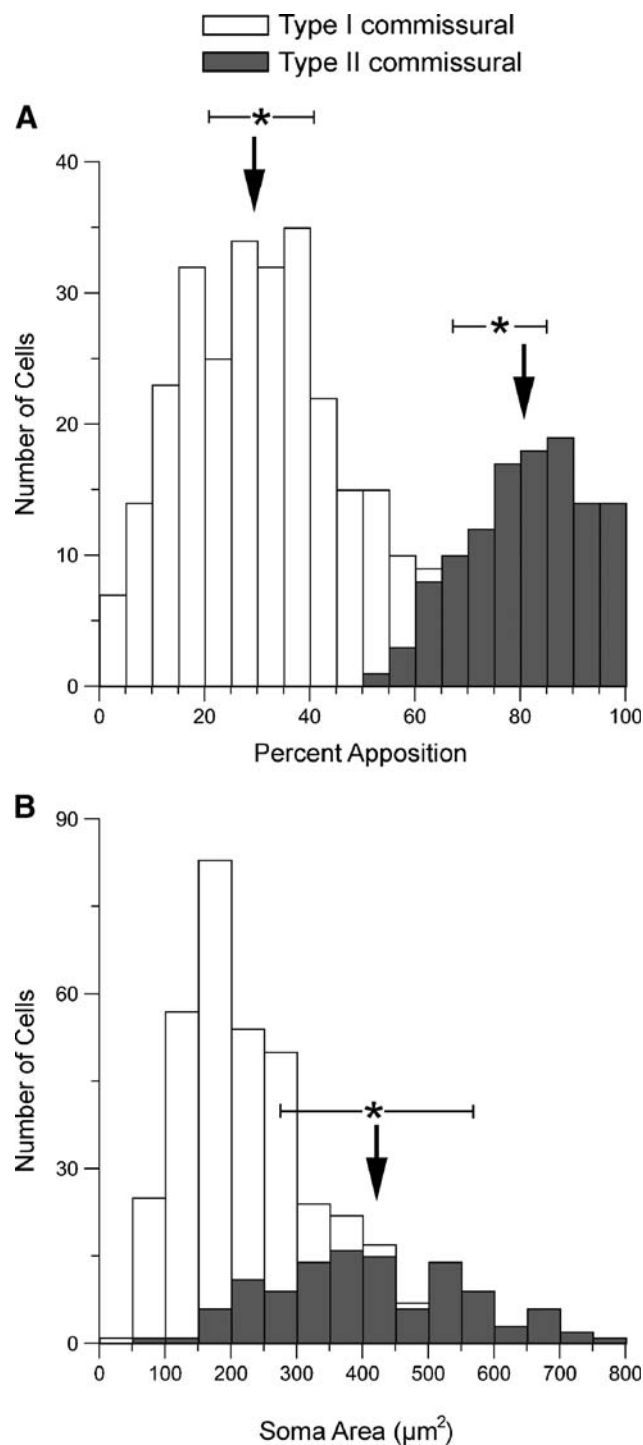


**FIG. 5.** Distributions of *Percent Apposition* and *Soma Area* for Types I and II neurons; **A** Histogram of PA scores. *Closed arrows* display the mean for the present sample of Type I ( $29 \pm 14\%$  (SD)) and Type II neurons ( $81 \pm 11\%$ ). *Asterisks and bars* show the mean  $\pm$  SD for Alibardi's (1998) sample of Types I ( $31 \pm 10\%$ ) and II ( $76 \pm 9\%$ ) neurons. **B** Histogram of SA scores; the histogram does not include two neurons with an SA greater than  $900 \mu\text{m}^2$ . *Closed arrow* displays the mean for the present sample of Type II neurons ( $419 \pm 162 \mu\text{m}^2$ ). *Asterisk and bars* shows the mean  $\pm$  SD for Doucet and Ryugo's (2006) sample of D-stellate or Type II multipolar neurons ( $418 \pm 140 \mu\text{m}^2$ ).

data of each rat (71% for rat 110705, 74% for rat 022306, and 58% for rat 090806). These findings were unexpected given previous descriptions (Alibardi 1998) that have reported an equally strong, but opposite Type II bias (47/70 neurons, 67%).

The disagreement between the two characterizations is almost certainly due to differences in sampling methods. The EM analyses of Alibardi (1998) required very thin sections (70 nm), making it impractical to examine all labeled commissural neurons in a chosen volume of tissue. Instead, representative sections were selected for complete analyses. Results may be skewed toward large cell bodies because discrete thin sections are more likely to miss small Type I somata than large Type II somata.

#### Topographical variations between Types I and II neurons

The VCN can be partitioned into a cytoarchitecturally distinct magnocellular core and a small cell cap. The magnocellular core contains the major classes of projection neurons. The small cell cap surrounds, or caps, the magnocellular core (Osen 1969). A growing

body of evidence suggests that the two subdivisions are not only structurally unique but also may subserve different auditory functions (Liberman 1991; Ghoshal and Kim 1997). The topographical distribution of Types I and II neurons within the VCN, therefore, provides important insights into the potential processing role of commissural projections.

One-half of the Type I neurons in the present study (131/261 neurons, 50%) were confined to a thin, 35- $\mu$ m shell within the small cell cap (Fig. 6). Type II neurons were rarely found there (4/116 neurons, 3%) and instead were scattered throughout the magnocellular core. The narrow demarcation of the shell area represents a conservative estimate of the ill-defined border between the magnocellular core and the small cell cap (Fig. 7). If the boundary of the shell region is doubled to 70  $\mu$ m, Type I neurons continue to outnumber Type II neurons by a 9:1 margin.

#### DISCUSSION

The present study was designed to test the hypothesis that Type I neurons form the largest component of

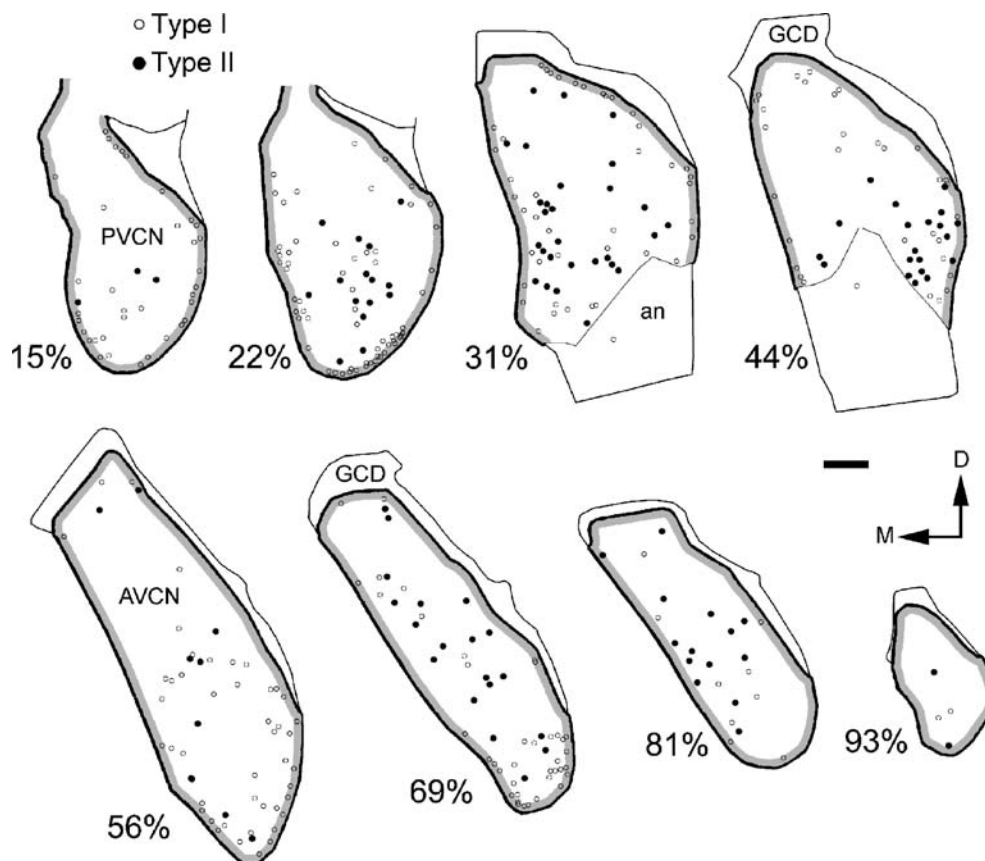


**FIG. 6.** Topographical distribution of Types I and II neurons; the drawings represent eight coronal sections through the VCN and display data from all three rats (0% equals posterior border of the cochlear nucleus). Each symbol represents one soma. Scale bar=200  $\mu$ m. GCD granule cell domain.



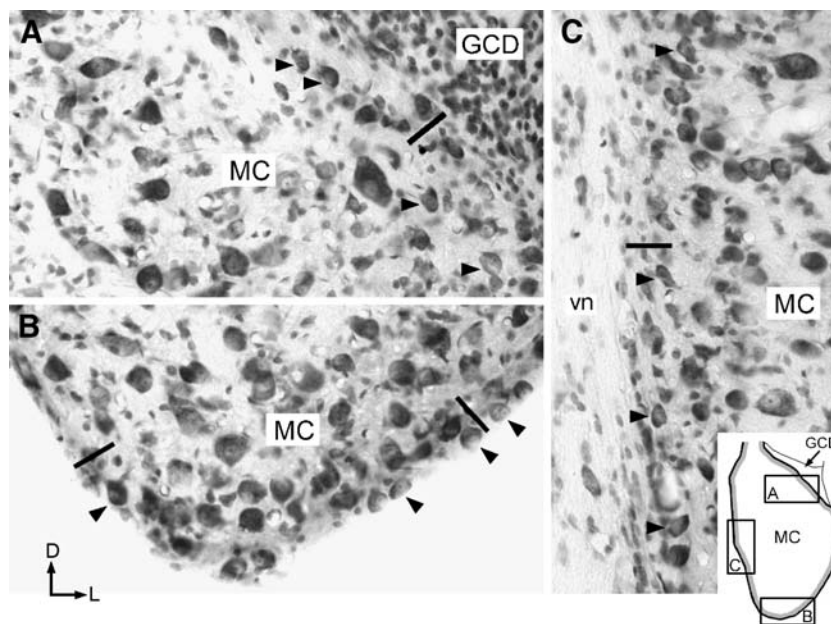


**FIG. 7.** Photomicrographs of the small cell cap in the rat VCN. Each panel displays Nissl-stained neurons in different regions of the posterior VCN (locations are indicated in a low-magnification drawing taken from Fig. 6A). In each panel, a 35- $\mu\text{m}$  scale bar marks the shell region containing high numbers of Type I neurons (gray

highlight in inset). **A** The border of the granule cell domain (GCD); **B** The free surface of the cochlear nucleus; **C** the vestibular nerve (vn); arrowheads point to small neurons that are found throughout the small cell cap.

the VCN commissure. This hypothesis was supported by results showing two Type I neurons for every Type II neuron in the commissure. It was also shown that the two classes of commissural neurons reside in different regions of the VCN. Most Type I neurons are located in the small cell cap, while Type II neurons are found almost exclusively in the magnocellular core. These observations call into question existing interpretations of commissural function that emphasize Type II projections from the magnocellular core. Our new perspectives on the neuronal composition of the commissure are summarized by the conceptual model in Figure 8.

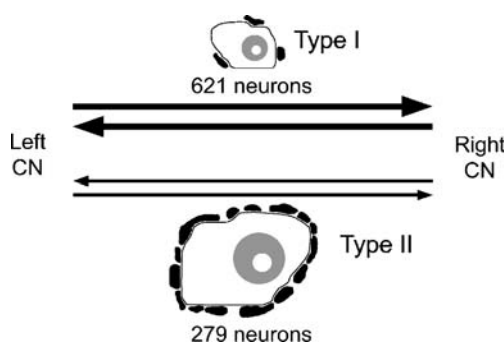


**FIG. 8.** Conceptual model of the VCN commissural pathway. Arrows indicate the relative strength and bidirectional nature of Types I and II projections. Anatomical illustrations depict differences in the soma size and axosomatic terminals of the two neural populations. The estimated number of each type is shown for one VCN, assuming that each VCN contains 900 commissural neurons.

These findings build upon previous descriptions of commissural neurons that have focused on soma size or axosomatic innervation. Shore and colleagues (1992) were the first to suggest a heterogeneous source for the commissural pathway to account for the variability that they observed in soma size. More recent surveys have demonstrated a preponderance of small and medium somata among commissural neurons and traced the smaller neurons to the small cell cap (Schofield and Cant 1996b; Doucet and Ryugo 2006). Alibardi (1998) subsequently introduced percent apposition as a method for separating commissural neurons into Types I and II morphologies. By combining these two morphological dimensions (i.e., SA and PA) into one system of classification, the present study offers a more rigorous definition of the neuronal types that contribute to the commissure, the relative number of each type, and their diverse topographical distributions within the VCN.

Our conclusions with respect to the relative number of Types I and II commissural neurons assume that they are retrogradely labeled in the same proportions as exist in vivo. Anterograde labeling suggests that commissural neurons have large and overlapping terminal fields (Shore et al. 1992; Schofield and Cant 1996a), making it unlikely that large injections favor labeling one type of neuron (Fig. 1). The most localized injection in the present study (Fig. 1, 110705) labeled the smallest number of commissural neurons but still yielded a Type I bias (Fig. 4).

Although the present study is based on considerably more commissural neurons than previous descriptions, the total volume of analyzed tissue represents less than 15% of the VCN. By contrast, Doucet and Ryugo (2006) sampled SA for commissural neurons obtained from over 50% of the VCN. Despite the considerable differences in the completeness of the samples, the resulting distributions are nearly identical. In the present study, SA scores ranged from 50 to 980  $\mu\text{m}^2$  (median=225  $\mu\text{m}^2$ ). In the Doucet and Ryugo study, they ranged from 49 to 838  $\mu\text{m}^2$  (median=218  $\mu\text{m}^2$ ). The close agreement between the independent datasets justifies the sampling strategy that was pursued in the present study.

### Functional considerations

The functional diversity of Types I and II commissural projections may be demonstrated by differences in their respective neurotransmitter systems. Type II neurons deliver glycinergic inhibition to the contralateral cochlear nucleus. Type I neurons almost certainly do not. Confirming prior work by Wenthold (1987), Alibardi (1998) reported that 45/106 (42%) commissural neurons were immunopositive for glycine. The remaining neurons (58%) were immunonegative for both glycine and GABA. If one assumes that Type II neurons are glycinergic and Type I neurons are nonglycinergic or nonGABAergic, the resulting Type I majority approaches the projection ratios that were observed in the present study (Fig. 8). Alibardi advanced his interpretation by directly linking neurochemistry to the ultrastructure of Types I and II neurons. However, he also described counterexamples of the basic pattern, such as a glycinergic Type I projection. Larger surveys are needed to determine the prevalence of these less common neural populations.

**Type II neurons may underlie fast inhibitory interactions between the cochlear nuclei.** Glycinergic inhibition is observed in the cochlear nucleus a few milliseconds after contralateral stimulation (Pfalz 1962; Mast 1970; Young and Brownell 1976; Evans and Zhao 1993; Joris and Smith 1998; Babalian et al. 1999, 2002; Shore et al. 2003; Needham and Paolini 2003; Davis 2005; Ingham et al. 2006). Type II neurons are one source of this short-latency binaural interaction (Needham and Paolini 2003; Arnott et al. 2004; Smith et al. 2005; Needham and Paolini 2006). This robust physiological phenomenon has encouraged conceptual interpretations of commissural communication that are dominated by Type II glycinergic inhibition.

Notwithstanding the rare glycinergic exception, Type I neurons are neither glycinergic nor GABAergic

(Alibardi 1998). Instead, Type I neurons may contribute to the short-latency excitation that is elicited by contralateral stimulation (Mast 1973; Young and Brownell 1976; Shore et al. 2003; Davis 2005; Needham and Paolini 2003; Ingham et al. 2006). Such effects are observed less frequently and are of smaller magnitude when compared with Type II inhibition. Consequently, Type I neurons do not appear to play a major role in fast interactions between the cochlear nuclei.

**Type I commissural neurons may underlie slow regulatory interactions between the cochlear nuclei.** Unilateral damage to the peripheral auditory system induces bilateral changes in the anatomical and physiological characteristics of cochlear nucleus neurons (Potashner et al. 1997; Suneja et al. 1998; Muly et al. 2002, 2004; Sumner et al. 2005; Rubio 2006). This plasticity may be induced by ossicular chain disruption, cochlea and auditory nerve ablation, or intense sound exposure. Although the VCN commissure has been implicated as the pathway mediating these adjustments, the fast inhibitory responses of Type II neurons are a poor substrate for long-term compensation. In light of our current findings, Type I neurons offer a more plausible mechanism for slow regulatory interactions between the cochlear nuclei.

The topography of Type I commissural neurons supports this hypothesized role. The small cell cap is emerging as a nexus of auditory brainstem regulatory pathways. Neurons that reside there are components of circuits that control the middle ear reflex (Billig et al. 2007) and cochlear output (Ye et al. 2000). The small cell cap is the preferred target of the collateral projections of medial olivocochlear neurons (Lieberman and Brown 1986; Brown et al. 1988; Benson et al. 1996), whose principal role is to modulate cochlear gain via their innervation of outer hair cells. Collectively, these connections implicate Type I commissural neurons as a principal component in a neural circuit that can regulate binaural sensitivity at the early stages of central auditory processing. Dynamic range adjustments directed by Type I projections would complement a similar binaural balancing that is achieved in the cochlea through the action of lateral olivocochlear inputs (Darrow et al. 2006). These slow regulatory interactions may optimize the processes that govern binaural directional hearing and effective listening in background noise.

In summary, our anatomical measures indicate that Type I projections from the small cell cap constitute at least two-thirds of the VCN commissure. These findings extend current views of commissure function that emphasize the fast, inhibitory influences of the Type II component. The parallel projections of the larger

Type I component may underlie slow, regulatory influences that enhance binaural processing or the recovery of function after injury.

## ACKNOWLEDGMENTS

This research was supported by NIH/NIDCD grants DC006268 and DC05211. The authors thank Elizabeth Jasolosky for technical help. The SV2 monoclonal antibody was developed by Kathleen Buckley and obtained from the Developmental Studies Hybridoma Bank. This important resource was developed under the auspices of the NICHD and is maintained by the University of Iowa, Department of Biological Sciences, Iowa City, IA 52242, USA.

## REFERENCES

- ALIBARDI L. Ultrastructural and immunocytochemical characterization of commissural neurons in the ventral cochlear nucleus of the rat. *Anat. Anz.* 180:427–438, 1998.
- ARNOTT RH, WALLACE MN, SHACKLETON TM, PALMER AR. Onset neurons in the anteroventral cochlear nucleus project to the dorsal cochlear nucleus. *J. Assoc. Res. Otolaryngol.* 5:153–170, 2004.
- BABALIAN AL, RYUGO DK, VISCHER MW, ROULLER EM. Inhibitory synaptic interactions between cochlear nuclei: evidence from an in vitro whole brain study. *Neuroreport* 10:1913–1917, 1999.
- BABALIAN AL, JACOMME AV, DOUCET JR, RYUGO DK, ROULLER EM. Commissural glycinergic inhibition of bushy and stellate cells in the anteroventral cochlear nucleus. *Neuroreport* 13:555–558, 2002.
- BAJJALIEH SM, FRANTZ GD, WEIMANN JM, McCONNELL SK, SCHELLER RH. Differential expression of synaptic vesicle protein 2 (SV2) isoforms. *J. Neurosci.* 14:5223–5235, 1994.
- BENSON TE, BERGLUND AM, BROWN MC. Synaptic input to cochlear nucleus dendrites that receive medial olivocochlear synapses. *J. Comp. Neurol.* 365:27–41, 1996.
- BENSON CG, GROSS JS, SUNEJA SK, POTASHNER SJ. Synaptophysin immunoreactivity in the cochlear nucleus after unilateral cochlear or ossicular removal. *Synapse* 25:243–257, 1997.
- BILLIG I, YEAGER MS, BLIKAS A, RAZ Y. Neurons in the cochlear nuclei controlling the tensor tympani muscle in the rat: A study using pseudorabies virus. *Brain Res.* 1154:124–136, 2007.
- BROOKE RE, ATKINSON L, EDWARDS I, PARSON SH, DEUCHARS J. Immunohistochemical localisation of the voltage gated potassium ion channel subunit Kv3.3 in the rat medulla oblongata and thoracic spinal cord. *Brain Res.* 1070:101–115, 2006.
- BROWN MC, LIBERMAN MC, BENSON TE, RYUGO DK. Brainstem branches from olivocochlear axons in cats and rodents. *J. Comp. Neurol.* 278:591–603, 1988.
- BUCKLEY K, KELLY RB. Identification of a transmembrane glycoprotein specific for secretory vesicles of neural and endocrine cells. *J. Cell. Biol.* 100:1284–1294, 1985.
- CANT NB. The fine structure of two types of stellate cells in the anterior division of the anteroventral cochlear nucleus of the cat. *Neuroscience* 6:2643–2655, 1981.
- CANT NB, GASTON KC. Pathways connecting the right and left cochlear nuclei. *J. Comp. Neurol.* 212:313–326, 1982.
- DARROW KN, MAISON SF, LIBERMAN MC. Cochlear efferent feedback balances interaural sensitivity. *Nat. Neurosci.* 9:1474–1476, 2006.
- DAVIS KA. Contralateral effects and binaural interactions in dorsal cochlear nucleus. *J. Assoc. Res. Otolaryngol.* 6:1–17, 2005.
- DOUCET JR, RYUGO DK. Projections from the ventral cochlear nucleus to the dorsal cochlear nucleus in rats. *J. Comp. Neurol.* 385:245–264, 1997.
- DOUCET JR, RYUGO DK. Structural and functional classes of multipolar cells in the ventral cochlear nucleus. *Anat. Rec. A Discov. Mol. Cell. Evol. Biol.* 288:331–344, 2006.
- DOUCET JR, ROSS AT, GILLESPIE MB, RYUGO DK. Glycine immunoreactivity of multipolar neurons in the ventral cochlear nucleus which project to the dorsal cochlear nucleus. *J. Comp. Neurol.* 408:515–531, 1999.
- EVANS EF, ZHAO W. Varieties of inhibition in the processing and control of processing in the mammalian cochlear nucleus. *Prog. Brain Res.* 97:117–126, 1993.
- GHOSHAL S, KIM DO. Marginal shell of the anteroventral cochlear nucleus: single-unit response properties in the unanesthetized decerebrate cat. *J. Neurophysiol.* 77:2083–2097, 1997.
- INGHAM NJ, BLEECK S, WINTER IM. Contralateral inhibitory and excitatory frequency response maps in the mammalian cochlear nucleus. *Eur. J. Neurosci.* 24:2515–2529, 2006.
- JANZ R, SUDHOF TC. SV2C is a synaptic vesicle protein with an unusually restricted localization: anatomy of a synaptic vesicle protein family. *Neuroscience* 94:1279–1290, 1999.
- JORIS PX, SMITH PH. Temporal and binaural properties in dorsal cochlear nucleus and its output tract. *J. Neurosci.* 18:10157–10170, 1998.
- LIBERMAN MC. Central projections of auditory-nerve fibers of differing spontaneous rate. I. Anteroventral cochlear nucleus. *J. Comp. Neurol.* 313:240–258, 1991.
- LIBERMAN MC, BROWN MC. Physiology and anatomy of single olivocochlear neurons in the cat. *Hear. Res.* 24:17–36, 1986.
- MAST TE. Binaural interaction and contralateral inhibition in dorsal cochlear nucleus of the chinchilla. *J. Neurophysiol.* 33:108–115, 1970.
- MAST TE. Dorsal cochlear nucleus of the chinchilla: excitation by contralateral sound. *Brain Res.* 62:61–70, 1973.
- MULY SM, GROSS JS, MOREST DK, POTASHNER SJ. Synaptophysin in the cochlear nucleus following acoustic trauma. *Exp. Neurol.* 177:202–221, 2002.
- MULY SM, GROSS JS, POTASHNER SJ. Noise trauma alters D-[3H] aspartate release and AMPA binding in chinchilla cochlear nucleus. *J. Neurosci. Res.* 75:585–596, 2004.
- NEALEN PM. An interspecific comparison using immunofluorescence reveals that synapse density in the avian song system is related to sex but not to male song repertoire size. *Brain Res.* 1032:50–62, 2005.
- NEEDHAM K, PAOLINI AG. Fast inhibition underlies the transmission of auditory information between cochlear nuclei. *J. Neurosci.* 23:6357–6361, 2003.
- NEEDHAM K, PAOLINI AG. Neural timing, inhibition and the nature of stellate cell interaction in the ventral cochlear nucleus. *Hear. Res.* 216, 217:31–42, 2006.
- OERTEL D, WU SH, GARB MW, DIZACK C. Morphology and physiology of cells in slice preparations of the posteroventral cochlear nucleus of mice. *J. Comp. Neurol.* 295:136–154, 1990.
- OLEN KK. Cytoarchitecture of the cochlear nuclei in the cat. *J. Comp. Neurol.* 136:453–482, 1969.
- PEALZ R. Centrifugal inhibition of afferent secondary neurons in the cochlear nucleus by sound. *J. Acoust. Soc. Am.* 34:1472–1477, 1962.
- POTASHNER SJ, SUNEJA SK, BENSON CG. Regulation of D-aspartate release and uptake in adult brain stem auditory nuclei after unilateral middle ear ossicle removal and cochlear ablation. *Exp. Neurol.* 148:222–235, 1997.
- RUBIO ME. Redistribution of synaptic AMPA receptors at glutamatergic synapses in the dorsal cochlear nucleus as an early response to cochlear ablation in rats. *Hear. Res.* 216, 217:154–167, 2006.
- SCHOFIELD BR, CANT NB. Origins and targets of commissural connections between the cochlear nuclei in guinea pigs. *J. Comp. Neurol.* 375:128–146, 1996a.

- SCHOFIELD BR, CANT NB. Projections from the ventral cochlear nucleus to the inferior colliculus and the contralateral cochlear nucleus in guinea pigs. *Hear. Res.* 102:1–14, 1996b.
- SHORE SE, GODFREY DA, HELFERT RH, ALTSCHULER RA, BLEDSOE SC, JR. Connections between the cochlear nuclei in guinea pig. *Hear. Res.* 62:16–26, 1992.
- SHORE SE, SUMNER CJ, BLEDSOE SC, LU J. Effects of contralateral sound stimulation on unit activity of ventral cochlear nucleus neurons. *Exp. Brain Res.* 153:427–435, 2003.
- SMITH PH, RHODE WS. Structural and functional properties distinguish two types of multipolar cells in the ventral cochlear nucleus. *J. Comp. Neurol.* 282:595–616, 1989.
- SMITH PH, MASSIE A, JORIS PX. Acoustic stria: anatomy of physiologically characterized cells and their axonal projection patterns. *J. Comp. Neurol.* 482:349–371, 2005.
- SUMNER CJ, TUCCI DL, SHORE SE. Responses of ventral cochlear nucleus neurons to contralateral sound following conductive hearing loss. *J. Neurophysiol.* 94:4234–4243, 2005.
- SUNEJA SK, POTASHNER SJ, BENSON CG. Plastic changes in glycine and GABA release and uptake in adult brain stem auditory nuclei after unilateral middle ear ossicle removal and cochlear ablation. *Exp. Neurol.* 151:273–288, 1998.
- WENTHOLD RJ. Evidence for a glycinergic pathway connecting the two cochlear nuclei: an immunocytochemical and retrograde transport study. *Brain Res.* 415:183–187, 1987.
- YE Y, MACHADO DG, KIM DO. Projection of the marginal shell of the anteroventral cochlear nucleus to olivocochlear neurons in the cat. *J. Comp. Neurol.* 420:127–138, 2000.
- YOUNG ED, BROWNELL WE. Responses to tones and noise of single cells in dorsal cochlear nucleus of unanesthetized cats. *J. Neurophysiol.* 39:282–300, 1976.